G-quadruplex Hydrogel-based Stimuli-responsive High-internal-phase Emulsion Scaffold for Biocatalytic Cascades and Synergistic Antimicrobial Activity

Sourav Das[1], Manju Solra[1], Jagabandhu Sahoo[2], Abhay Srivastava[1], Fathima S[1], Mrinmoy De[2] & Subinoy Rana*[,1]

[1]Materials Research Centre, Indian Institute of Science, Bangalore 560012, India

[2]Organic Chemistry, Indian Institute of Science, Bangalore 560012, India

*Corresponding Author: Dr. Subinoy Rana

Email ID: subinoy@iisc.ac.in

Graphical Abstract/TOC

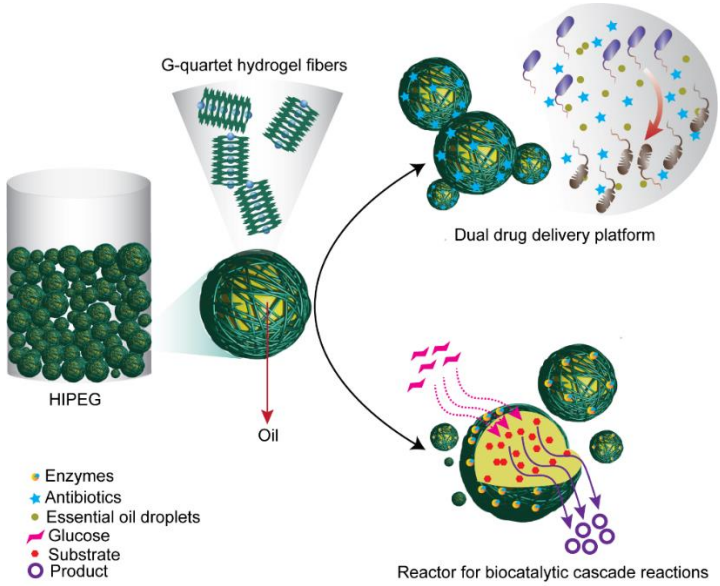

ABSTRACT

High internal phase emulsions (HIPEs) are non-equilibrium systems with distorted liquid droplet shapes consisting of high volume of internal phase (>74% v/v), enabling high loading of pharmaceutics and useful viscoelastic properties. Stability of the HIPEs is low and requires a high volume of surfactants in the continuous phase, which is environmentally unfriendly. Utilization of hydrogel as the continuous phase to stabilize HIPEs would offer a robust method to produce stable HIPE gels displaying reconfigurable and biocompatible properties, as well as access the huge repertoire of different biocompatible hydrogels. Herein, we introduce a new gel-immobilized HIPE (HIPEG) using chiral G-quadruplex (GQ) based hydrogel with external stimuli-responsive dual-drug release behavior, which is scarce for HIPEs. The hydrophilic and hydrophobic compartments of HIPEGs allow encapsulation of different drugs in both the compartments, with stimuli-responsive diffusion mediated release. Encapsulation of natural oils and antibiotics produces synergistic antimicrobial effects on both Gram positive (MRSA) and Gram negative (*P. aeruginosa*) bacterial strains. Moreover, we demonstrate biocatalytic reaction networks utilizing compartmentalized enzyme dyads. Notably, the ideal viscoelastic property of HIPEGs enables 3D bioprinting into different shapes, making the scaffold potential for tissue engineering applications. Altogether, our approach offers a one-step route to stimuli-responsive HIPE microcompartments immobilized in GQ hydrogels with endogenous reactivity and high viscoelasticity, and provides a viable step towards the development of biocompatible soft materials with tailorable functionality.

1. INTRODUCTION

High internal phase emulsions (HIPEs) are highly concentrated emulsions with an internal phase volume fraction (Φ) exceeding 0.74.[1] Owing to their unique flow behavior, semi-solid texture, and large interfacial area, HIPEs have received significant interest in multiple areas, including food,[2] cosmetic,[3] pharmaceutical,[4] and petroleum industries.[5] Besides, the high fraction of oil content in a HIPE system enables the encapsulation of large volumes of water-immiscible therapeutics, providing an ideal platform for drug delivery applications. Likewise, the water and oil phases allow simultaneous immobilization of hydrophilic and hydrophobic cargoes, achieving efficient dual therapeutic delivery and biphasic catalytic transformations.[6,5] Moreover, polymerization of the external continuous phase and extraction of the internal dispersed phase results in a light-weight porous structure, which modulates the physical properties of HIPEs and expands the repertoire of their applications. These hierarchical porous materials have been effectively utilized in diverse applications such as

tissue engineering,[7] wound dressing,[8] sensing,[9] and energy storage.[10] Adaptable HIPEs with responsiveness to multiple external stimuli would further make these systems amenable to designing intelligent soft materials.[11]

The fabrication of stable HIPEs poses a significant challenge due to the higher fraction of the dispersed phase, resulting in non-equilibrium emulsion droplets with deformation of the thermodynamically stable spherical shape.[12] Various strategies have been adopted to stabilize the out-of-equilibrium system through covalent and non-covalent modification of the continuous phase.[13,14] A common approach uses surfactants for stabilization, but the amount of surfactant required is very high (5-50 wt%) for effective HIPEs, causing negative environmental impacts.[15] To curtail the usage of hazardous surfactants, numerous efforts are focused on creating substitute emulsifiers that would stabilize the droplets through minimizing the surface tension. Solid particles have been utilized to stabilize emulsions, also known as Pickering emulsions, which is dependent on the wettability of the particles and hence, carefully designed surface chemistry.[16] Pickering emulsion based HIPEs with stimuli responsiveness is challenged with complex synthetic protocols. A potential alternative to stabilize the non-equilibrium droplet shape is provided by gelation of the continuous phase using polymers, proteins, and low molecular weight gelators, packing the droplets efficiently within the continuous phase.[17–22] HIPE droplets dispersed in in-situ gelled continuous phase provide functional micro-compartments mimicking tissues. However, the introduction of hydrogels as the continuous phase to produce a HIPE gel (HIPEG) would offer functionally encoded systems with external stimuli sensitiveness and biocompatibility. In fact, immobilization of spatially distributed synthetic microcompartments such as porous microbeads, liposomes, and polymersomes in three-dimensional (3D) hydrogels have provided great opportunities for enhanced catalysis,[23] tissue engineering, drug delivery,[24] and construction of prototissues.[25] Functionally programmed hydrogels can be molded and combined into higher-order assemblies using 3D printing and regulated crosslinking, paving the way for the production of soft modular materials. These strategies have mostly been used to print cell-laden hydrogels from hydrogelators such as silk fibroin and hyaluronic acid.[26,27]

Herein, we introduce a new strategy to fabricate HIPEGs using G-quadruplex (GQ) based hydrogel as a continuous phase for 3D immobilization of extremely concentrated dispersion of oil droplets, providing a stimuli-responsive soft-matter microreactor. The GQ hydrogel fibers stabilize various types of oil microdroplets with a volume fraction as high as 0.85, which are stable for months at room temperature. Similar to the DNA GQ structures having specific functions in the genome, these GQ hydrogels offer a biocompatible platform

for antibacterial,[28] drug delivery,[29] 3D bioinks,[30] and wound healing[31] applications. Liquid droplet immobilized gels have been recently used in multiple biological applications as microcompartments capable of RNA and protein catalysis,[32] *in vitro* gene expression,[33] artificial predations and trafficking,[34] controlled electric field excitation,[35] and nitric-oxide-induced vasodilation.[36] Given the wide varieties of biomimetic activity of these platforms, we immobilized dispersed populations of edible/natural oil microdroplets containing sequestered therapeutics, enzymes, and substrates. These loaded HIPEGs are employed as a microreactor for biocatalytic reactions in which the oil soluble product is easily isolated. The HIPEG framework also serves as a depot for the simultaneous encapsulation of water-immiscible and miscible antibiotics that exhibit synergistic antimicrobial effects on Gram positive and Gram negative strains. Moreover, the GQ hydrogel is formed by non-covalent supramolecular interactions that impart multiple stimuli-responsiveness, including temperature, pH, glucose, and peroxide, which is translated into the HIPEG platform. Owing to the fluidity of the droplets, applied strain causes additional deformation of the shape and hence highly elastic property. We observed that the GQ HIPEG exhibit high viscoelasticity and injectability that has been exploited to construct higher order structures by 3D bioprinting into different complex shapes.[37] Overall, GQ based HIPEGs gels can be transformed into porous scaffolds, printable materials, dual therapeutic delivery scaffold, and as efficient biocatalytic microreactors.

2. RESULTS AND DISCUSSION

2.1 Synthesis of Hydrogel via G-quartet Assembly

An efficient emulsifier for the preparation of HIPEs should stabilize >74% of the internal phase without causing a phase reversion. We utilized a biocompatible hydrogel emulsifier based on self-assembled guanosine nucleobase quartets. Guanosine assembles into GQ through hydrogen bonding between the guanine groups templated by K^+ ions.[38] Formation of boronate ester between the *cis*-diol on ribose sugars of GQs and phenylboronic acid (PBA) in the presence of KOH results in a stable hydrogel (Fig. 1a). The GQ hydrogel is transparent with a transmittance of ~90% (Fig. 1b). These GQ conjugates stack over, forming columnar fibrous structure and crosslinked networks through π-π stacking interactions.[39,38] To confirm the π-stacking of G-quartets in the hydrogel, we used Thioflavin-T (ThT) that intercalates into hydrophobic region of an assembly. The fluorescence intensity of ThT is significantly enhanced in GQ hydrogel matrix than in aqueous solution (Fig. S1). Powder X-ray diffraction (PXRD) analysis further validated the formation of GQ and the secondary structure of the

hydrogel. The Bragg's diffraction peak at 2θ = 3.64 in the PXRD spectrum corresponds to a characteristic interlayer distance of *d* = 24.25 Å (Fig. S2).[29] A peak at 26.83 (*d* = 3.32 Å) represents the *π*-*π* stacking distance between two planar G-quartets.[39] In addition, the circular dichroism (CD) spectrum of GQ hydrogel shows two positive bands at ~230 nm and 290 nm with a negative band at 255 nm (Fig. S3).[30] The CD signature indicates that the G-quartets assemble in both head-to-tail and head-to-head orientations in the hydrogel.[30,40]

The formation of boronate ester was confirmed using Fourier-transform infrared spectroscopy (FTIR) and ^{11}B NMR studies. In the FTIR spectra, stretching vibration at 1098 cm^{-1} accounts for the formation of B-O-C bond (Fig. S4). In addition, the C-O-H vibration peak at 1080 cm^{-1} of guanosine and B-O-H band at 1340 cm^{-1} of PBA disappears upon formation of the GQ hydrogel.[41] The new B-O-C peak in the GQ hydrogel and the disappearance of the B-O-H and C-O-H peaks of PBA and guanosine, respectively, suggest the formation of cyclic boronate ester bonds (B-O-C) in the GQ hydrogel network.[42] Further, the amide vibration of guanosine at 1726 cm^{-1} shifts to 1687 cm^{-1} in the GQ hydrogel (Fig. S4) due to intermolecular hydrogen-bonding between the G-quartets.[42,43] In the ^{11}B NMR spectra, there was only one sharp peak at 28.56 ppm for PBA, which is attributed to free boronic acid group (Fig. 1c). The peak shifted to 6.37 ppm after hydrogelation, suggesting a different chemical environment around boron atoms due to boronate bond formation.[30] FESEM image clearly shows a fibrous morphology of the hydrogel and the average cross-sectional area of a single fiber is ~20 nm (Fig. S5). The fibrous nature of the GQ hydrogel is also observed in the AFM images (Fig. 1d and Fig. S6). These observations support the formation of G-quadruplex hydrogel by the supramolecular stacking of G-quartets. It is worth noting that the GQ hydrogels are extremely compact, with extraordinarily interpenetrated tightly packed fibers. Moreover, the fraction of water content in the GQ hydrogel is 0.98.

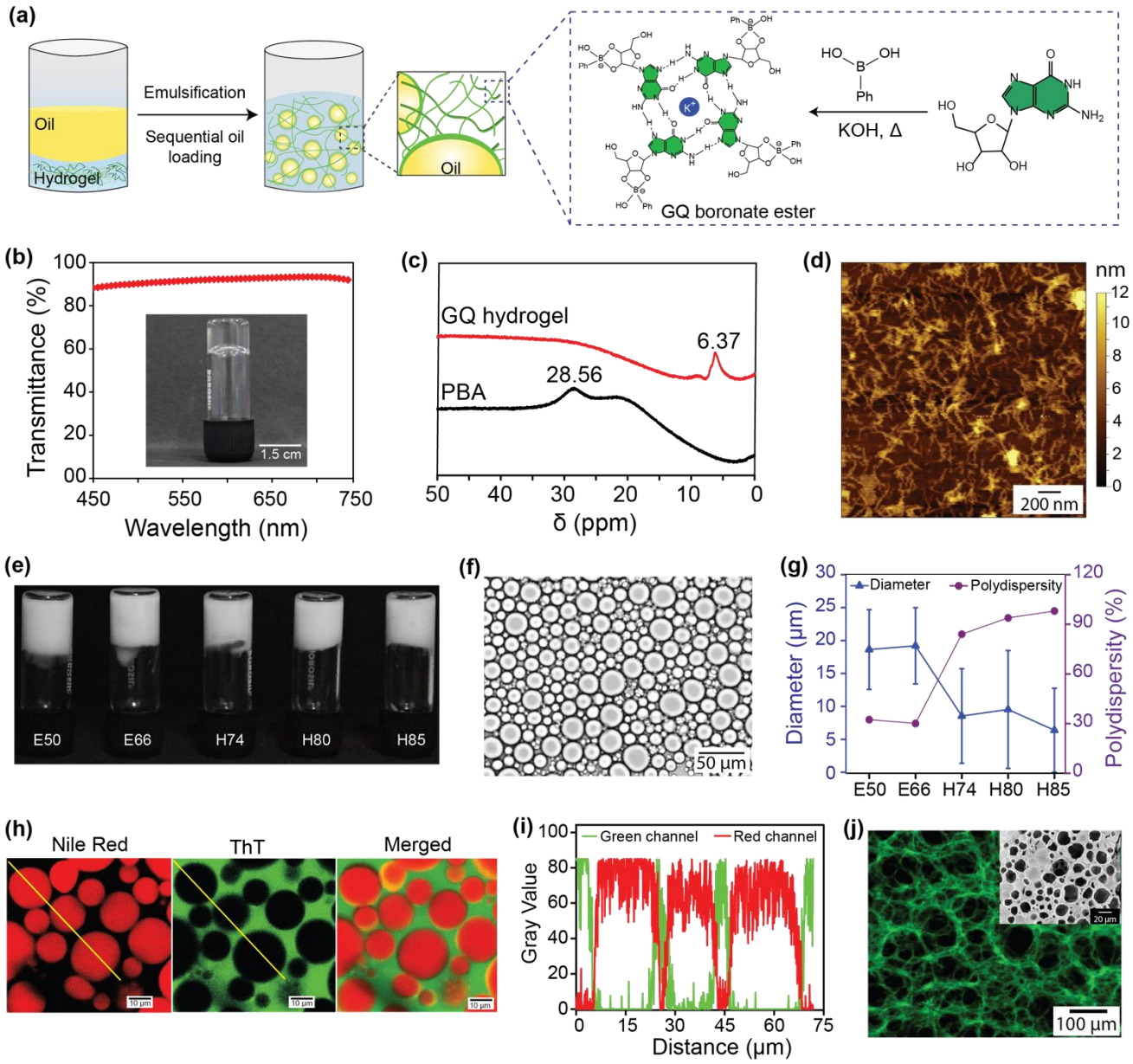

Fig. 1. (**a**) A schematic showing fabrication of emulsion gels and HIPEGs with the structure of G quartet forming hydrogel. The oil is placed on top of the hydrogel, followed by emulsification with a homogenizer to produce stable emulsion gels and HIPEGs. (**b**) Transmittance trace of GQ hydrogel along with a photograph in an inverted vial. (**c**) ^{11}B NMR spectra of GQ hydrogel and PBA. (**d**) AFM image of the fibrous nature of GQ hydrogel. (**e**) Visual appearance of the emulsion gels and HIPEGs loaded with different percentages of oil (n-decane) in glass vials of diameter 1.5 cm each, recorded by a digital camera. (**f**) Optical microscopic image of H80 system, where the oil loading is 80%. (**g**) The diameter and polydispersity of different emulsion gels and HIPEGs, determined using ImageJ software. E50, E66 are emulsion gels, whereas H74, H80 and H85 are HIPEGs. (**h**) CLSM images of H80, where the GQ hydrogel and n-decane are stained with green (ThT) and red fluorescent (nile red) dyes, respectively. (**i**) Line intensity profile obtained from (**h**) for nile red and ThT, analyzed using ImageJ software. The Gray values were determined along the yellow traces shown in (**h**). (**j**) Fluorescence image of ThT dye loaded H80 dried in air for 1 h showing the fibrillar network around empty pores created by evaporation of the oil droplets. The inset shows a FESEM image of H80 after drying in open air for 1 h.

2.2 Fabrication of GQ Hydrogel-based High Internal Phase Emulsions

We prepared HIPEs by emulsifying an oil phase into GQ hydrogel as schematically illustrated in Fig. 1a. Fibrillar networks of the hydrogel provide the continuous phase, which interacts with the dispersed oil droplets leading to stabilized HIPEs. Initially, the emulsions were prepared by loading n-decane as the oil at different ratios of 50, 66, 74, 80, and 85 % (v/v) into the GQ hydrogel. We term the 50 and 66 % as emulsion gels (E50 and E66, respectively) and beyond that as high internal phase emulsion gels, HIPEGs (H74, H80 and H85). The HIPEGs were prepared *via* two step homogenization process to minimize phase segregation.[17] A series of stable HIPEGs upto 85 % oil loading are formed with a homogenous appearance (Fig. 1e) without any noticeable phase separation. The optical image of the HIPEG shows closely packed emulsion droplets dispersed in the continuous gel phase (Fig. 1f). Moreover, the average diameter of the emulsion droplets decreased significantly from ~18 μm in E50 and E66 to ~7 μm for oil loadings ≥74 % (Fig. 1g), which resembles a trend similar to that reported for other HIPEs.[17,22] However, the polydispersity of the emulsion gels increases significantly as 74 % oil fraction was reached, resulting in high packing density. Furthermore, increased crowding and decreased interparticle distance between the oil droplets was observed for increasing oil percentages (Fig. S7). However, the continuous hydrogel network prevents coalescence of neighboring oil droplets.

We carried out confocal laser scanning microscopy (CLSM) analysis to examine the microstructure and the shape of emulsions formed. The oil phase was stained by nile red, while the GQ gel was loaded with ThT. It is clear from the CLSM images that red fluorescent oil microdroplets were surrounded by a layer of GQ hydrogel emitting green fluorescence (Fig. 1h and Fig. S8). The green fluorescence on the outer surface and red in the inner core exhibited a high optical contrast, indicative of a droplet compartmentalized microstructure. The fluorescence intensity profile along the green and red channels of the CLSM images showed the interstitial spaces between the droplets covered by the GQ gel since the green fluorescence intensity increases and red becomes negligible at the intersections (Fig. 1i). The confocal images of the HIPEGs with increasing oil percentages showed increased crowding by polydispersed oil droplets beyond the high-internal phase limit (Fig. S9). It should be noted that the maximum volume packing fraction of 0.74 is geometrically feasible for similar sized spheres.[12] Hence, HIPEs are generally stabilized through deformation of oil droplets. However, in contrast to the traditional HIPEs with deformation of droplets into polyhedral shapes, GQ hydrogel stabilized HIPEGs showed no significant change in the droplet shape even at 80% oil fraction. The high oil loading rather results from the increased polydispersity

of the droplet sizes (Fig. 1g). The high polydispersity with oil percentages beyond the threshold produces smaller droplets that fit in the interstitial spaces between larger emulsions, leading to efficient packing in the HIPEGs.

Imaging of the dried HIPEGs showed ThT-labelled interconnected hydrogel fibers with voids corresponding to the oil droplets (Fig. 1j). Furthermore, evaporation of the n-decane phase caused the H80 to deform into a polyhedral morphology after 1 h exposure to open air, as observed in the FESEM image (*inset* Fig. 1j). The FESEM analysis of H80 shows a porous morphology of the HIPEG and confirms the presence of a GQ hydrogel on the surface of oil droplets (*inset* Fig. 1j).

2.3 Viscoelastic Properties of HIPEG

The HIPEGs are resistant to flow upon inversion of the vial (Fig. 1e) and did not break down in excess water, indicating the stiffness of the material. However, the HIPEG scaffold exhibits ductility when forced to flow. The ductile behavior was demonstrated through stirring H80 at 1700 rpm at room temperature for 1 h, generating fluidic emulsions without oil release or phase inversion (Fig. S10) that arises from the transient disruption of the fibrous structure.[44] The H80 microstructure remains intact with similar droplet sizes after the stirring. Dynamic rheological measurements provided insight into the mechanical strength of the HIPEGs. The angular frequency sweep experiments shown in Fig. 2a and Fig. S11 suggest viscoelastic nature of the emulsion gels at different percentages of oil loading. All the HIPEGs showed an elastic behavior as the storage modulus (G') values were always greater than the loss modulus (G") within the range of oscillation frequencies investigated (Fig. S11). Interestingly, the G' and G" values were enhanced as the oil fraction was increased. However, the G' and G" moduli were unaffected by the increasing shear frequency. Therefore, the elasticity coupled with the frequency independence suggests the HIPEs to exhibit typical gel-like behavior with modular strength.[19] The increase in G' is attributed to a denser packing of oil droplets within the continuous phase, which enhances inter-particle interactions and GQ hydrogel network elasticity. Moreover, the complex shear modulus (G*) of the emulsions was elevated as the oil percentage increased, indicating higher stiffness. As seen from Fig. 2b, HIPEGs exhibit G* ranging from 0.37 kPa (H74) to 3.97 kPa (H85) spanning the mechanical properties exhibited by human brain tissue and intestine, respectively, making them potential for biomaterial construction.[45] Besides, the porous structure produced by water evaporation at room temperature maintained the structural integrity, with interconnected hydrogel fibers adsorbed on the droplet surface. The strength of the HIPEGs depend on the hydrogel layer wrapping around the network of micron sized pores as observed in the FESEM image of a

lyophilized sample (Fig. S12). Given the significantly low content of GQ fibers in H80 porous structure, the material becomes extremely light (*inset* of Fig. S12).

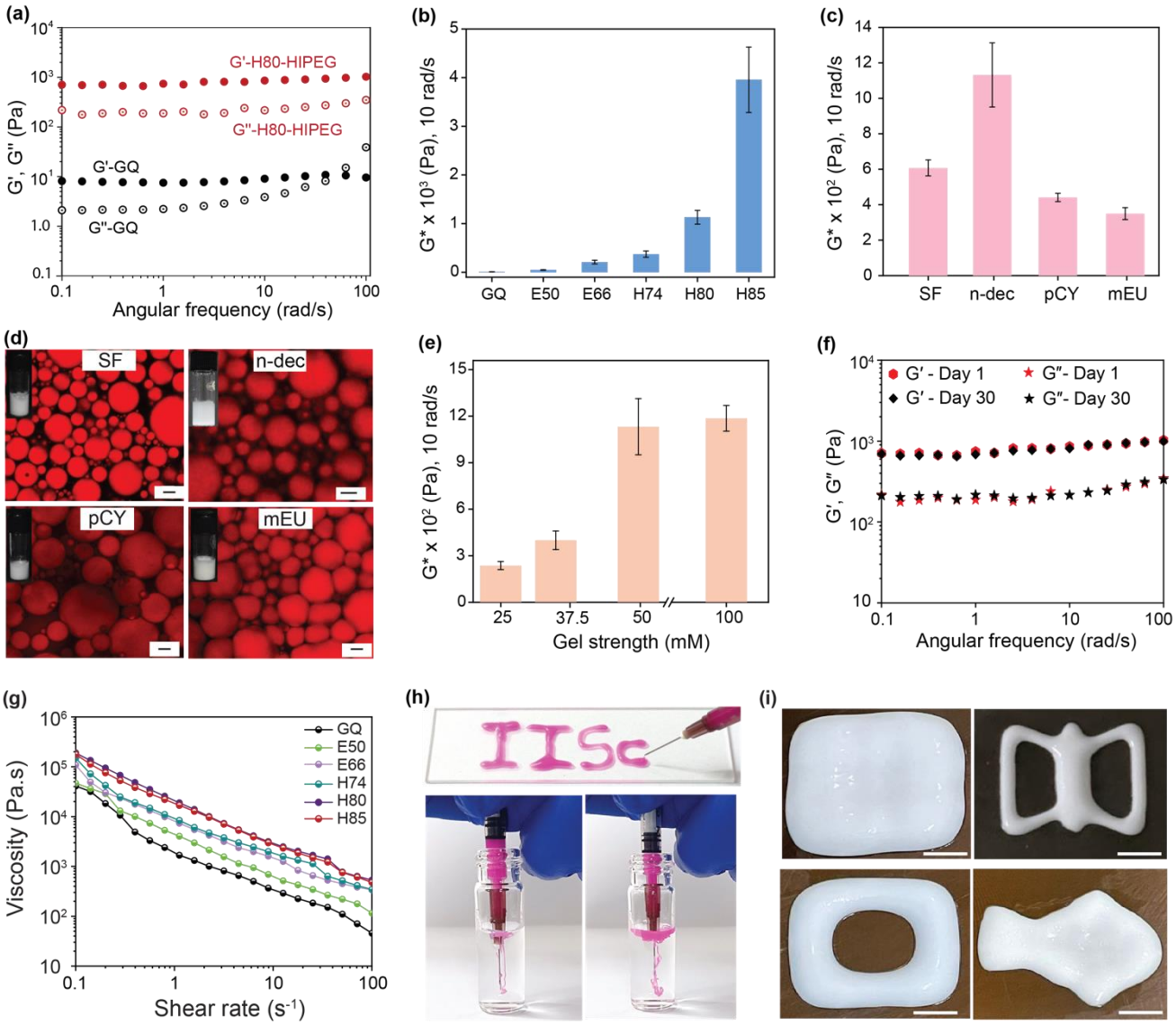

Fig. 2. (**a**) Variation in the moduli of GQ hydrogel and H80. The storage (G′) and loss (G″) moduli are indicated with filled and unfilled symbols, respectively. (**b**) Complex shear modulus (G*) of the emulsion gels (E50, E66) and the HIPEGs (H74, H80, H85) at 10 rad/s. (**c**) Complex shear modulus (G*) H80 at 10 rad/s for different oils: sunflower oil (SF), n-decane (n-dec), p-cymene (pCY) and methyl eugenol (mEU). (**d**) Confocal images of SF, n-dec, p-CY, and mEU loaded H80 along with their corresponding photographs in the inset, respectively. The oil is stained with nile red. Scale bar: 10 µm (**e**) Complex shear modulus of H80 prepared with different strengths of the GQ hydrogel (25, 35, 50, and 100 mM). (**f**) Moduli variation of the H80 at day 1 and day 30 with angular frequency. The HIPEGs were stored at room temperature with sealed cap. (**g**) Shear thinning behaviour of emulsion gels and HIPEGs using n-decane as the oil. (**h**) Digital photographs of injectable H80 stained with $DiIC_{18}$ dye on a glass slide (*upper panel*) and water inside a glass vial (*lower panel*). The H80 was loaded in a 1 mL syringe. (**i**) Different 3D printed shapes using H80 containing sunflower oil. The scale bar is 1 cm for all the 3D shapes.

We explored the versatility of the approach to encapsulate different oils in GQ hydrogel. Different edible and antibacterial oils such as sunflower oil (SF), p-cymene (pCY) and methyl eugenol (mEU) were used to fabricate HIPEGs, which would find utility in practical applications.[46,47] The H80 containing SF, pCY and mEU showed similar elastic behavior to that of n-decane, exhibiting greater G' values than G" within 0.1 – 100 rad/s oscillation frequency (Fig. S13). The stiffness of the H80 system containing SF, pCY and mEU varied depending on the oil type as observed by the complex shear modulus (Fig. 2c). The droplet shapes of these H80 systems showed interesting trend among the oils. It was observed through CLSM imaging that SF oil containing HIPEG had high polydispersity, pCY had droplets with larger diameter, and mEU showed distorted polyhedral shapes (Fig. 2d). Further, we examined the role of GQ hydrogel content in modulating the strength of H80 using 25, 35 and 100 mM GQ hydrogels. The droplet size of H80 made of 35 mM GQ gel were much larger compared to that of 100 mM, where well-dispersed oil droplets could be observed (Fig. S14). However, 25 mM GQ gel based H80 started oiling off as soon as it was taken out from the vial. Rheology measurements showed that the G* and G' values increase with the increasing strength of the GQ hydrogel (Fig. 2e and Fig. S15). These observations indicate that the stiffness of H80 is tunable by varying the strength of the GQ hydrogel. For practical applications, the storage stability of HIPEGs over time is a key factor. We observed that H80 remain stable for at least a month when stored at room temperature without oiling off or coalescence (Fig. S16). Also, the HIPEGs retained the mechanical properties of the as-prepared samples (Fig. 2f), indicating robust structural stabilization of the droplets. The prolonged stability of the HIPEGs, even at 80% (v/v) oil, is primarily due to the interconnected fibrillar network of the continuous phase that wrap around the dispersed oil droplets, restricting their movement and coalescence.[28,48]

2.4 Utility of the HIPEGs in 3D Printing

Injectable emulsions consisting of biocompatible materials provide effective systems for developing tissue constructs and drug screening scaffolds. The rheological properties of HIPEGs indicate a facile shear thinning behavior as the viscosity decreases with increasing shear rate from 0.1-100 s^{-1} (Fig. 2g), which is ideal for fabricating injectable materials.[49] Interestingly, the viscosity increased with the percentage of oil loading up to 80% due to the reduced interparticle distance and interdroplet friction, which tend to restrict the droplet flow.[17] The increased viscosity along the whole shear-thinning curve indicates a more rigid GQ hydrogel network with increasing oil loading. It is noteworthy that this interesting flow behavior is typically observed in emulsion gels, in contrast to traditional concentrated emulsions.[17] The

shear-thinning behavior of other oil containing H80 such as SF also shows a similar trend (Fig. S17). Next, we tested the injectability of the HIPEG by loading 1,1'-dioctadecyl-3,3,3',3'-tetramethylindocarbocyanine perchlorate ($DiIC_{18}$) dye-labelled H80 containing SF in a syringe. The H80 scaffold showed excellent writable property (*upper panel* of Fig. 2h), as well as injectability without any blockage or collapse (*lower panel* of Fig. 2h). Therefore, the H80 offers the prospect of fabricating 3D printed scaffold for the delivery of hydrophobic as well as hydrophilic therapeutic molecules. Given the injectability of the HIPEG, we explored the 3D printability using a bioprinter. We used H80 loaded with SF oil for printing the 3D structures. As shown in Fig. 2i, 3D shapes bearing different curvatures and complex shapes were printed with high fidelity. It should be noted that the HIPEG is stabilized by GQ-hydrogel at a concentration as low as 0.4 % (w/v), which is considerably lower than other gel-based bioinks (normally >5 wt%).[50] This extremely low content of GQ solids in H80 results in higher fluidity, enabling superior printability of the HIPEG system. As the emulsion gels fabricated here contains guanosine, a biocompatible and bioactive ingredient,[51] a strategy for therapeutic testing, tissue engineering, food manufacturing and 3D printed food could be foreseen.[7,22,52]

2.5 Stimuli Responsiveness of the HIPEGs

Responsive materials that change their physicochemical state by different external stimuli present adaptable and intelligent materials for diverse applications including catalysis,[53,54] tissue engineering,[55] drug delivery,[56] and related biomedical fields.[57] Given the numerous on-field applications of HIPEs, stimuli-responsive properties of these materials would introduce effective adaptable systems, which is scarce till date. The present HIPEGs exhibit responsiveness due to sensitivity of GQ-based gel systems to different stimuli such as temperature, glucose, pH, and crown ether. First, we tested the reversibility of H80 by varying the temperature in a range of 25-70 °C. Demulsification of H80 occurs as the temperature is raised above a threshold (Fig. 3a), which is supported by the reduction in turbidity (Fig. 3b) at 500 nm where the system does not absorb. The H80 is stable up to 40 °C, above which it starts to break down and completely demulsifies above 50 °C (Fig. 3a-b). This phase transition occurs due to the breakdown of hydrogen bonding interactions between the guanosine moieties in the GQ hydrogel at higher temperatures, such that the layer surrounding the oil droplets is destroyed. Temperature cycling between 60 °C and room temperature allows complete demulsification and emulsification efficiently without fatigue (Fig. 3c). Notably, the reversibility of the H80 system could be achieved even after 10 cycles,

and the microstructure as well as size of the H80 remains almost similar over the cycles (Fig. S18). Therefore, the temperature-sensitive GQ hydrogel fibers impart effective thermo-responsiveness to the HIPEGs, making them amenable to practical applications. In addition, we examined pH as a stimulus for the H80 system using a fluorescent dye, Rhodamine B (RhB), release. Fig. 3d shows that as the pH is lowered to 4.0, the release of RhB is higher (~ 31 %) compared to the control but when the pH is further lowered down to 2.0, the H80 system gets completely demulsified and a rapid release of RhB is observed (Fig. S19). The demulsification happens because lowering the pH breaks the hydrogen bonds between the guanosines forming G-quartets in the GQ hydrogel, thus dissolving the layer surrounding the oil droplets in H80.[28,29]

Next, we evaluated the effect of a chemical stimulus, glucose, by quantifying the release of RhB loaded in the GQ gel prior to emulsification. Glucose breaks the gel by competitive binding with the cyclic boronate ester of the GQ hydrogel that stabilizes the oil droplets.[29] It is evident that increasing glucose concentration leads to a faster release of RhB from the H80 (Fig. 3e). At 50 mg/mL of glucose, the H80 system completely demulsifies, releasing >95 % RhB to the aqueous solution upon 60 min incubation (Fig. S20). In contrast, the control experiment without glucose showed ~10-fold slower release of RhB at 60 min in buffer, and the H80 can be seen floating on the surface of the aqueous glucose solution (Fig. S20). To assess the potential of HIPEG for glucose-responsive drug delivery, we constructed functional H80 with β-carotene and doxorubicin (DOX) as model hydrophobic and hydrophilic drugs, respectively. DOX was incorporated in the GQ hydrogel matrix prior to emulsification, whereas hydrophobic β-carotene in sunflower oil. As shown in Fig. 3f, increasing the concentration of glucose results in faster cargo release. At 50 mg/mL of glucose, approximately 87 % and 90 % of DOX and β-carotene is released in 120 min, which is approximately 8 times higher compared to that of the controls without glucose (~11 % for DOX and ~12 % for β-carotene). In addition, the drug release kinetics was found to depend on the glucose concentrations (Fig. S21 a-b). Therefore, a synergistic benefit of emulsion and hydrogel is harnessed from HIPEGs by encapsulating both hydrophilic and hydrophobic drugs in the continuous and dispersed phase, respectively. Also, the chemical stimuli responsiveness and the HIPEG's high loading capacity for hydrophobic molecules helps circumvent the challenges typically encountered with drug release and loading efficiency of hydrophobic molecules in drug delivery systems.[58,59]

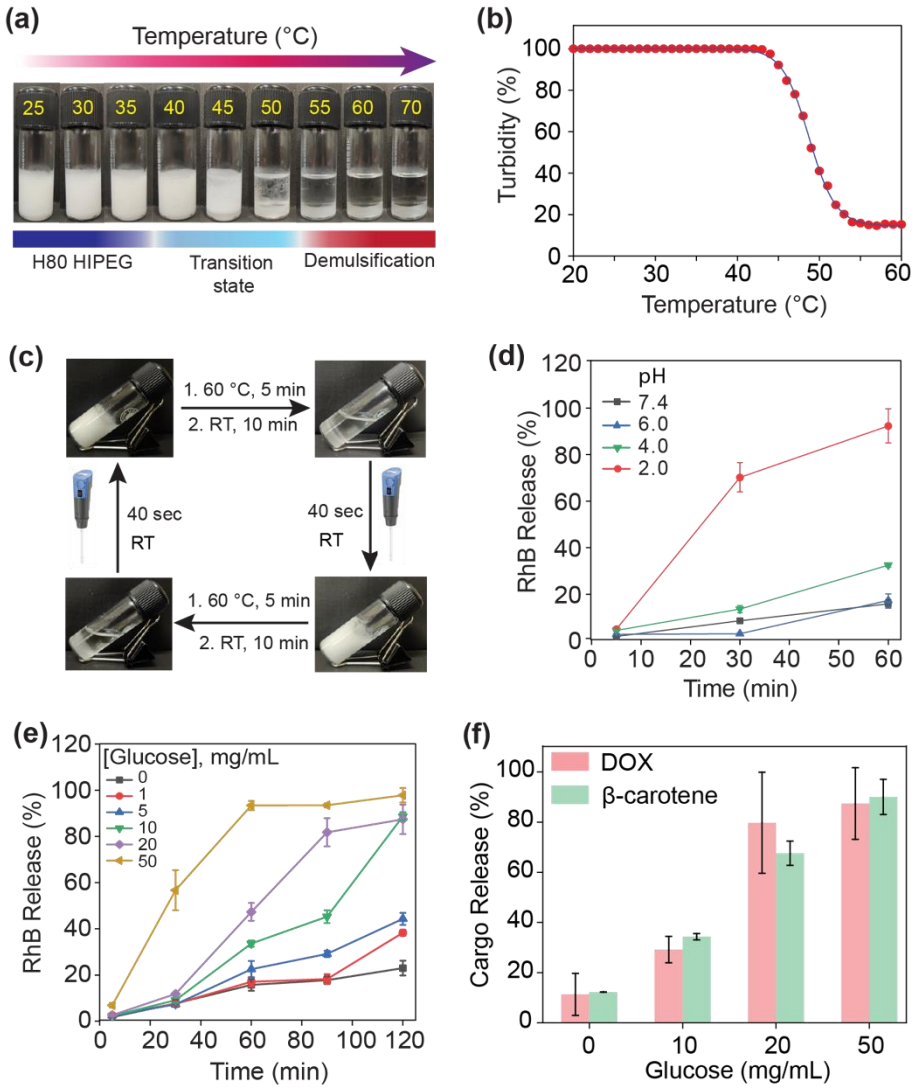

Fig. 3. (**a**) Digital photographs of H80 HIPEG upon increasing temperature. The H80 vial was immersed in water bath for 5 min at each temperature. Demulsification of the system is depicted by the separation of the oil and GQ hydrogel phase. (**b**) Variation in turbidity at 500 nm of H80 with the increase in temperature during the demulsification process. (**c**) Photographs of the reversible emulsification/demulsification process of H80 (**d**) Effect of pH on the release of RhB from H80 containing the dye in the hydrogel. (**e**) Effect of different concentrations of glucose on the release of RhB from H80 containing the dye in the GQ hydrogel. The lines are drawn to guide the eye. (**f**) Glucose responsive cargo release from the sunflower oil-based H80 as a function of glucose concentration after 120 min. The release of DOX and β-carotene were measured by collecting the absorbance at 480 nm and 452 nm, respectively.

We have also studied the release of cargoes without any stimuli over long period of time using reported protocol.[60] As observed in Fig. S22, the release of DOX reaches about 65 % by 12 h and then maintains a steady release kinetics until 48 h. Similarly, for β-carotene we observe that the release is quite slow (~25 %) in 12 h, which then maintains steady kinetics till 48 h. The faster release kinetics of DOX compared to β-carotene from H80

originates presumably from the direct contact of the release medium (phosphate buffer pH 7.4) with the continuous phase in which DOX is encapsulated. The β-carotene release is quantified by collecting the diffused cargo into n-hexane phase. The release of β-carotene is slow because of the strong interconnected GQ hydrogel fibrils retarding the transport of β-carotene through the oil droplet surface by generating a higher diffusion resistance.[60] The other factor that limits the faster release of β-carotene is attributed to the chemical potential difference between sunflower oil and hexane for the diffusion of β-carotene from the internal phase H80 to the outside phase.[61] However, the tunability of dual cargo release by diffusion and external stimuli presents a great platform for designing effective drug delivery systems.

2.6 HIPEG as an Efficient Microreactor of Biocatalytic Reaction Networks

Complex cellular systems are functional through efficient multiple biocatalytic transformations, often involving cascade reaction networks.[62] The spatial confinement and templation of enzyme pairs in the nano- or microscale compartments leads to superior catalytic reactions with higher selctivity.[63,64] Despite the efficacy of biphasic catalysis in allowing environmentally benign separation of catalyst and products into separate immiscible phases, the reaction is often restricted by the limited organic/aqueous interfacial area.[65] We anticipated that the greater specific surface area coupled with the microcompartments of HIPEGs and biocompatibility of the gel phase would produce more efficient bio-catalysis than a traditional surfactant-stabilized emulsion system.[53] To validate the hypothesis, two enzymes, glucose oxidase (GOx) and horseradish peroxidase (HRP), were entrapped in the hydrogel followed by emulsification with 1-decanol (oil) containing 4-chloro-1-naphthol (4-CN). As illustrated through CLSM imaging, when H80 was loaded with green fluorescent FITC-labelled GOx (GOx-FITC) and red fluorescent RITC-labelled HRP (HRP-RITC) at 5:1 ratio, both the enzymes were localized at the oil microdroplet interface (Fig. 4a). GOx oxidizes glucose to generate H_2O_2, which is consumed by HRP to oxidize 4-CN into a purple-colored oil-soluble product 4-chloro-1-naphthon (4-CNO) (Fig. 4b). It can be seen from Fig. 4c that addition of glucose to H80 generates a purple-colored product, indicating the oxidation of 4-CN to 4-CNO. The product 4-CNO is oil soluble, which was easily separated by centrifugation and analyzed using UV-vis spectroscopy. Control experiments indicated that a single enzyme could not trigger the biocatalytic cascade reactions (Fig. 4d and Fig. S23). Fig. 4e shows the increase in absorbance maximum at 560 nm corresponding to the 4-CNO product at different time intervals of the two-enzyme cascade process. Therefore, the biocatalytic cascade proceeds only when both enzymes are confined within the continuous phase of H80. Notably,

the biocatalytic cascade reaction does not proceed without emulsification (Fig. 4f-g), signifying the importance of the large surface area of the oil droplets covered by the enzyme immobilized GQ hydrogel. Besides, the higher local concentration of the enzyme pair promotes the biocatalytic cascade reaction. We further checked the stability of the GOx/HRP pair over time by monitoring the oxidation of 4-CN to 4-CNO. It was readily observed that the enzyme pair performed the cascade reaction with more than >95% efficiency even after seven days (Fig. 4h), indicating that H80 helps maintaining the native activity of the enzymes. Overall, our HIPEG system provides an efficient microreactor for reaction networks with biphasic reaction compartments that would have important biotechnological and medicinal uses.

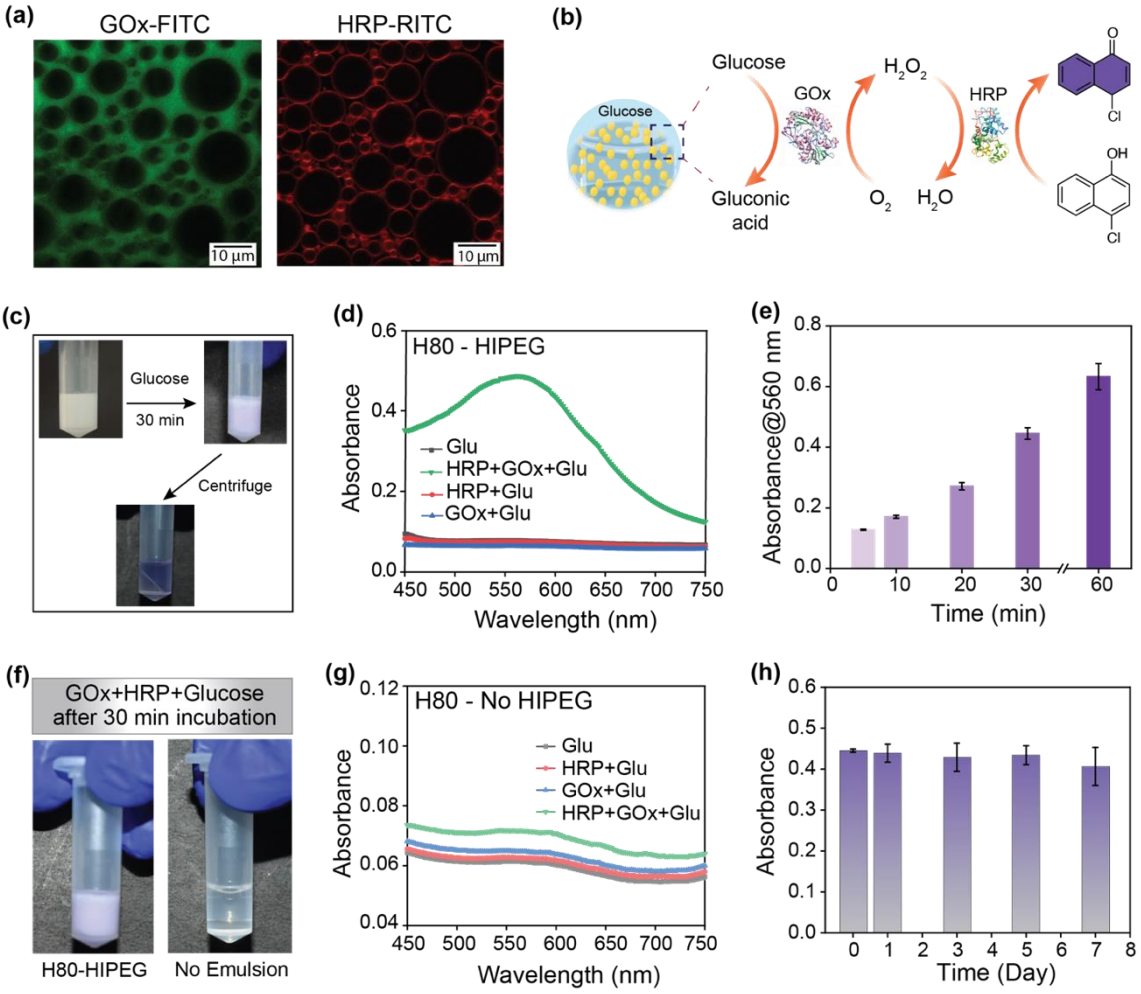

Fig. 4. (**a**) CLSM image of H80 system where the continuous phase is embedded with fluorescein isothiocyanate (FITC) labelled GOx and rhodamine B isothiocyanate (RITC) labelled HRP. (**b**) Schematic of the GOx/ HRP cascade reaction for the oxidation of 4-chloro-1-naphthol (4-CN) to 4-chloro-1-naphthon (4-CNO). GOx-catalyzed oxidation of glucose to produce H_2O_2, followed by 4-CN HRP-catalyzed oxidation of 4-CN to a purple color oil soluble product (4-CNO). (**c**) Emulsification of GQ hydrogel (loaded with GOx/HRP couple) with 1-decanol (containing 4-CN) leads to the formation of H80 which facilitates the production of a purple product when glucose is

added on top of the H80 system. (**d**) Time dependent increase in the purple 4-CNO product from the oxidation of 4-CN driven by the two enzyme (GOx/HRP) cascade reaction within the H80 system, as shown by the absorbance at 560 nm of 4-CNO at 25 °C. (**e**) Absorption profile of the control experiments depicting the oxidation of 4-CN to 4-CNO after 30 min of incubation at 25 °C. The product formation occurs only in the presence of GOx/HRP couple in the H80 system. (**f**) Digital photographs of the comparison between the biocatalytic reaction in H80 system without emulsification and with emulsification. (**g**) Control experiments showing that without H80 the biocatalytic reaction does not proceed after incubation of 30 min. (**h**) Stability of the GOx/HRP couple inside H80 over a period of 7 days determined by the oxidation of 4-CN to 4-CNO upon addition of glucose 30 min prior to recording the spectrum.

2.7 HIPEG for Synergistic Combination Therapy Against Microbial Strains

Combination therapy presents a complementary strategy for the treatment of microbial infections by enhancing the efficacy of therapeutics to overcome drug resistance.[66,67] Synergistic effects of drug combinations produce greater effectiveness and overcome limitation associated with a single drug.[68] Combination of antibiotics and essential oils have been shown to exert synergistic effects against bacterial strains.[69] Notably, the HIPEGs provide an ideal platform for combination drug therapy owing to its ability to encapsulate both hydrophobic and hydrophilic drugs. We utilized the H80 scaffold encapsulating antibacterial p-cymene (p-Cy) oil and hydrogel-loaded common antibiotics to evaluate the antimicrobial efficacy. We hypothesized that the gradual release of p-Cy and the antibiotic would ensure constant and localized concentration of the dual drugs for the effective killing of bacterial strains. We tested *in vitro* antibacterial efficacy of H80 against two model bacterial strains, Gram positive (MRSA) and Gram negative (*P. aeruginosa*) *via* an agar plate diffusion assay. To test the dual antibacterial efficacy of H80 scaffold against MRSA, the hydrogel phase was loaded with vancomycin (VC), whereas ciprofloxacin (Cip) was used for *P. aeruginosa.* We observe that HIPEG containing VC and PC separately show an observable zone of inhibition (ZOI) against MRSA, which increases significantly when VC and PC are encapsulated within the same H80 (Fig. 5a and 5b). Specifically, the ZOI of H80 containing both VC and PC against MRSA was 16.5 mm (S3), which is significantly higher than only VC (9.5 mm, S1) and PC (6.0 mm, S2). The GQ gel containing vancomycin showed lesser ZOI. The control studies were carried out without emulsification, and it was observed that none of the controls could show a similar effect to that of H80 containing both PC and VC (Fig. S24a-b). Similarly, the antibacterial efficacy of the H80 scaffold against *P. aeruginosa* showed that the combination of p-cymene and ciprofloxacin (P3) slightly enhanced the antibacterial efficacy of the H80 scaffold with ZOI (23.75 mm) as compared to only ciprofloxacin loaded H80 (ZOI 20 mm) and PC (2 mm) (Fig. 5c and 5d). The control studies are shown in Fig. S24c-d. These

results validate the efficacy of HIPEGs as a potential scaffold for the realization of the benefit of two therapeutics within one system.

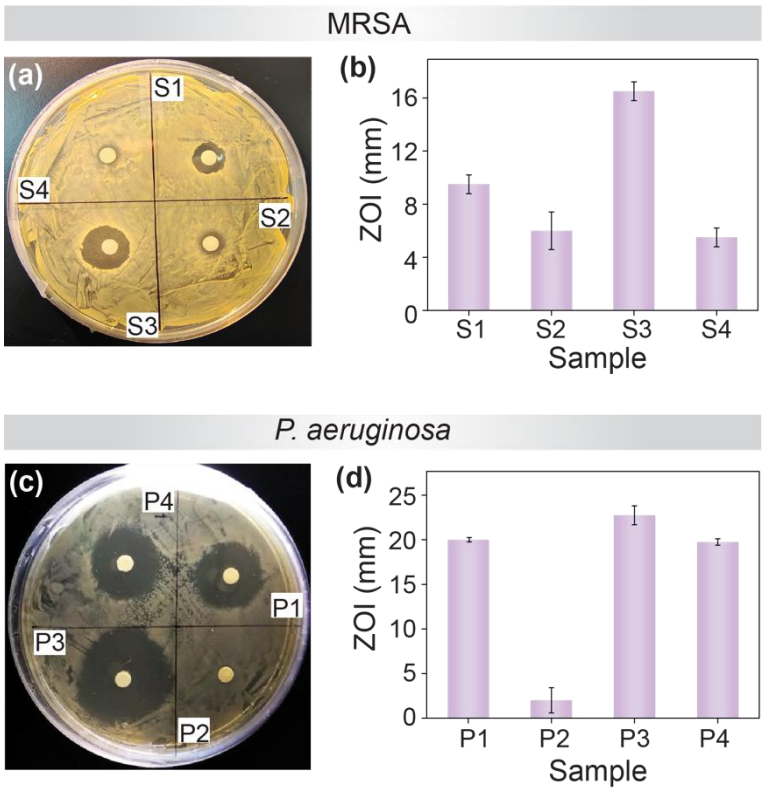

Fig. 5. Antibacterial activity of vancomycin (VC) and p-Cy (oil) loaded H80 against MRSA (**a**) and their corresponding zone of inhibition (ZOI) (**b**). S1: H80 with VC, sunflower oil loaded. S2:H80 loaded with p-cymene. S3: H80 loaded with VC and p-Cy. S4: GQ gel with VC. Antibacterial activity of ciprofloxacin (Cip) and p-cymene (oil) loaded H80 against *P. aeruginosa* (**c**) and their corresponding ZOI (**d**). P1: H80 with Cip, sunflower oil loaded. P2:H80 loaded with p-Cy. P3: H80 loaded with Cip and p-Cy. P4: GQ gel with Cip.

3. CONCLUSIONS

We demonstrate an approach to construct HIPEGs stabilized by guanosine hydrogels that provides effective microreactors encapsulating drug molecules with varied solubilities and enzymes. The driving force for stabilization of the emulsion gels originates from the interconnected GQ hydrogel fibers in the continuous phase that covers the oil droplet surface, restricting droplet movement and coalescence, even with an internal volume fraction as high as 85% (v/v). Rheological measurements indicate high viscoelastic and shear thinning behaviors of the HIPEGs similar to the GQ hydrogel, enabling the bioprinting of different 3D shapes containing the microreactors. A notable aspect of the HIPEGs is their responsiveness to multiple stimuli such as heat, pH, and glucose. While elevated temperatures above 37 °C

disrupts the HIPEG allowing the complete separation of the aqueous and organic phases, re-emulsification reproduces the HIPEG with similar viscoelastic properties. Furthermore, we demonstrate tunable release profile of dual cargoes – a hydrophilic drug in GQ hydrogel and a hydrophobic provitamin in the oil droplets – using glucose and pH as the stimuli. The presence of hydrogel layer on the HIPEG surface has been exploited for the encapsulation of antagonistic enzymes HRP/GOx to catalytically oxidize its substrate in a cascade whose product is oil soluble and can be purified easily through centrifugation. The HIPEG provided longer stability to the enzymes as well as enhanced the catalytic reaction. Furthermore, the hydrophobic and hydrophilic compartments of HIPEG allowed encapsulation of common antibiotics and essential oils, realizing synergistic effect of dual therapeutic against Gram-positive and Gram-negative bacterial strains. Thus, the capability to encapsulate both hydrophilic and hydrophobic therapeutic payloads provide new prospects for the development of HIPEG systems as novel biocarriers for enhanced efficacy. Thus, the design and application of stimuli-responsive HIPEGs comprising of biocompatible nucleosides will be the focus of future research on *in vivo* activity. Given the promising results of our HIPEG system, in the long term, it should attract huge interest in advancing the simple approach to produce more complicated stimuli-responsive HIPEG materials for applications in bioengineering, medicine, and bio-catalysis.

SUPPORTING INFORMATION: Materials, methodology, detailed experimental procedures: preparation of hydrogel, HIPEGS and their characterization using fluorescence emission, CD, FTIR, ^{11}B-NMR, PXRD and AFM, optical and confocal imaging. Procedure for stimuli responsive behavior of H80 HIPEG, cumulative drug release, and antimicrobial activities. Data corresponding to characterization of GQ hydrogel and HIPEGs, storage stability, ductility, stimuli responsiveness, biocatalytic cascade reactions, dual drug release, antimicrobial activities, standard curves for doxorubicin and β-carotene.

NOTES

The authors declare no competing financial interest.

ACKNOWLEDGEMENTS

S.R. acknowledges financial support from Science and Engineering Research Board (ECR/2018/00255). The authors are thankful to the Department of Science and Technology (DST-FIST: SR/FST/PSII009/2010) for the instrumental facility at MRC. M.S. is thankful to UGC for the doctoral fellowship. A.S. and F.S. are thankful to MoE for the doctoral fellowship.

Financial support from the DBT-RA Program in Biotechnology and Life Sciences (Award No: DBT-RA/2021/January/NE/231) is gratefully acknowledged by S.D. We thank Smarak I. Chaudhury for helping with the manuscript.

REFERENCES

1. Cameron, N. R. High internal phase emulsion templating as a route to well-defined porous polymers. *Polymer (Guildf).* **46**, 1439–1449 (2005).
2. Li, X. *et al.* High Internal Phase Emulsion for Food-Grade 3D Printing Materials. *ACS Appl. Mater. Interfaces* **12**, 45493–45503 (2020).
3. Watanabe, K., Ohmura, T., Ikeda, T., Miki, A. & Teshigawara, T. Hyper internal phase W/O emulsion stabilized with a specific surfactant that forms an anomalous bicontinuous cubic liquid crystal. *Int. J. Cosmet. Sci.* **32**, 315–316 (2010).
4. Speltini, A. *et al.* Carbon nanotubes-modified poly-high internal phase emulsions for pharmaceuticals pre-concentration and determination. *J. Pharm. Biomed. Anal.* **207**, 114391 (2022).
5. Bizmark, N., Du, X. & Ioannidis, M. A. High Internal Phase Pickering Emulsions as Templates for a Cellulosic Functional Porous Material. *ACS Sustain. Chem. Eng.* **8**, 3664–3672 (2020).
6. Rodriguez, A. M. B. & Binks, B. P. Catalysis in Pickering emulsions. *Soft Matter* **16**, 10221–10243 (2020).
7. Aldemir Dikici, B. *et al.* Thiolene-and Polycaprolactone Methacrylate-Based Polymerized High Internal Phase Emulsion (PolyHIPE) Scaffolds for Tissue Engineering. *Biomacromolecules* **23**, 720–730 (2022).
8. McGann, C. L., Streifel, B. C., Lundin, J. G. & Wynne, J. H. Multifunctional polyHIPE wound dressings for the treatment of severe limb trauma. *Polymer (Guildf).* **126**, 408–418 (2017).
9. Zhao, C., Danish, E., Cameron, N. R. & Kataky, R. Emulsion-templated porous materials (PolyHIPEs) for selective ion and molecular recognition and transport: applications in electrochemical sensing. *J. Mater. Chem.* **17**, 2446–2453 (2007).
10. Brun, N. *et al.* Hard Macrocellular Silica Si(HIPE) Foams Templating Micro/Macroporous Carbonaceous Monoliths: Applications as Lithium Ion Battery Negative Electrodes and Electrochemical Capacitors. *Adv. Funct. Mater.* **19**, 3136–3145 (2009).
11. Das, S., Solra, M. & Rana, S. Emulsion Gel: a Dual Drug Delivery Platform for Osteoarthritis Treatment. *Regen. Eng. Transl. Med.* (2022) doi:10.1007/s40883-022-00282-x.
12. Cameron, N. R. & Sherrington, D. C. High Internal Phase Emulsions (HIPEs) - Structure, Properties and Use in Polymer Preparation. in *Advances in Polymer Science* vol. 126 162–214 (Springer New York, 1996).
13. Kovačič, S., Preishuber-Pflügl, F., Pahovnik, D., Žagar, E. & Slugovc, C. Covalent incorporation of the surfactant into high internal phase emulsion templated polymeric

foams. *Chem. Commun.* **51**, 7725–7728 (2015).

14. Chen, Y. *et al.* High internal phase Pickering emulsions stabilized by tannic acid-ovalbumin complexes: Interfacial property and stability. *Food Hydrocoll.* **125**, 107332 (2022).

15. Sun, G., Li, Z. & Ngai, T. Inversion of Particle-Stabilized Emulsions to Form High-Internal-Phase Emulsions. *Angew. Chemie Int. Ed.* **49**, 2163–2166 (2010).

16. Yang, X.-C. *et al.* Drug Delivery Using Nanoparticle-Stabilized Nanocapsules. *Angew. Chemie* **123**, 497–501 (2011).

17. Zhu, Y. *et al.* High Internal Phase Oil-in-Water Pickering Emulsions Stabilized by Chitin Nanofibrils: 3D Structuring and Solid Foam. *ACS Appl. Mater. Interfaces* **12**, 11240–11251 (2020).

18. Dickinson, E. Emulsion gels: The structuring of soft solids with protein-stabilized oil droplets. *Food Hydrocoll.* **28**, 224–241 (2012).

19. Ono, F., Shinkai, S. & Watanabe, H. High internal phase water/oil and oil/water gel emulsions formed using a glucose-based low-molecular-weight gelator. *New J. Chem.* **42**, 6601–6603 (2018).

20. Carranza, A. *et al.* Nonaqueous Synthesis of Macroporous Nanocomposites Using High Internal Phase Emulsion Stabilized by Nanohydroxyapatite. *Adv. Mater. Interfaces* **4**, 1700094 (2017).

21. Horowitz, R. *et al.* Highly efficient and tunable miktoarm stars for HIPE stabilization and polyHIPE synthesis. *Polymer (Guildf).* **217**, 123444 (2021).

22. Wang, L.-S. *et al.* Porous Polymerized High Internal Phase Emulsions Prepared Using Proteins and Essential Oils for Antimicrobial Applications. *Langmuir* (2022) doi:10.1021/ACS.LANGMUIR.2C01565.

23. Liu, J. *et al.* Hydrogel-Immobilized Coacervate Droplets as Modular Microreactor Assemblies. *Angew. Chemie Int. Ed.* **59**, 6853–6859 (2020).

24. Gao, W. *et al.* Hydrogel containing nanoparticle-stabilized liposomes for topical antimicrobial delivery. *ACS Nano* **8**, 2900–2907 (2014).

25. Liu, S. *et al.* Signal processing and generation of bioactive nitric oxide in a model prototissue. *Nat. Commun. 2022 131* **13**, 1–12 (2022).

26. Park, K. M. *et al.* In situ supramolecular assembly and modular modification of hyaluronic acid hydrogels for 3D cellular engineering. *ACS Nano* **6**, 2960–2968 (2012).

27. Li, S. *et al.* A Silk Fibroin Methacryloyl-Modified Hydrogel Promoting Cell Adhesion for Customized 3D Cell-Laden Structures. *ACS Appl. Polym. Mater.* **4**, 7014–7024 (2022).

28. Hu, J. *et al.* Stimuli-Responsive Hydrogels with Antibacterial Activity Assembled from Guanosine, Aminoglycoside, and a Bifunctional Anchor. *Adv. Healthc. Mater.* **9**, 1–8 (2020).

29. Li, Y. *et al.* A G-Quadruplex Hydrogel via Multicomponent Self-Assembly: Formation and Zero-Order Controlled Release. *ACS Appl. Mater. Interfaces* **9**, 13056–13067 (2017).

30. Biswas, A. *et al.* Arylboronate esters mediated self-healable and biocompatible dynamic G-quadruplex hydrogels as promising 3D-bioinks. *Chem. Commun.* **54**, 1778–1781 (2018).

31. Li, Y. *et al.* A Guanosine-Quadruplex Hydrogel as Cascade Reaction Container Consuming Endogenous Glucose for Infected Wound Treatment—A Study in Diabetic Mice. *Adv. Sci.* **9**, 2103485 (2022).

32. Drobot, B. *et al.* Compartmentalised RNA catalysis in membrane-free coacervate protocells. *Nat. Commun. 2018 91* **9**, 1–9 (2018).

33. Aufinger, L. & Simmel, F. C. Artificial Gel-Based Organelles for Spatial Organization of Cell-Free Gene Expression Reactions. *Angew. Chemie Int. Ed.* **57**, 17245–17248 (2018).

34. Qiao, Y., Li, M., Booth, R. & Mann, S. Predatory behaviour in synthetic protocell communities. *Nat. Chem. 2016 92* **9**, 110–119 (2016).

35. Yin, Y. *et al.* Non-equilibrium behaviour in coacervate-based protocells under electric-field-induced excitation. *Nat. Commun. 2016 71* **7**, 1–7 (2016).

36. Liu, S. *et al.* Enzyme-mediated nitric oxide production in vasoactive erythrocyte membrane-enclosed coacervate protocells. *Nat. Chem. 2020 1212* **12**, 1165–1173 (2020).

37. Lee, M. C., Tan, C., Ravanfar, R. & Abbaspourrad, A. Ultrastable Water-in-Oil High Internal Phase Emulsions Featuring Interfacial and Biphasic Network Stabilization. *ACS Appl. Mater. Interfaces* **11**, 26433–26441 (2019).

38. Davis, J. T. & Davis, J. T. G-Quartets 40 Years Later: From 5′-GMP to Molecular Biology and Supramolecular Chemistry. *Angew. Chemie Int. Ed.* **43**, 668–698 (2004).

39. Peters, G. M. *et al.* G4-quartet·M+ borate hydrogels. *J. Am. Chem. Soc.* **137**, 5819–5827 (2015).

40. Peters, G. M. *et al.* A G4·K+ hydrogel stabilized by an anion. *J. Am. Chem. Soc.* **136**, 12596–12599 (2014).

41. Bhattacharyya, T. *et al.* Cytidine-Derived Hydrogels with Tunable Antibacterial Activities. *ACS Appl. Bio Mater.* **2**, 3171–3177 (2019).

42. Ghosh, T., Biswas, A., Gavel, P. K. & Das, A. K. Engineered Dynamic Boronate Ester-Mediated Self-Healable Biocompatible G-Quadruplex Hydrogels for Sustained Release of Vitamins. *Langmuir* **36**, 1574–1584 (2020).

43. Li, J. *et al.* A multifunctional self-healing G-PyB/KCl hydrogel: smart conductive, rapid room-temperature phase-selective gelation, and ultrasensitive detection of alpha-fetoprotein. *Chem. Commun.* **55**, 7922–7925 (2019).

44. Yan, T. *et al.* Widely Adaptable Oil-in-Water Gel Emulsions Stabilized by an Amphiphilic Hydrogelator Derived from Dehydroabietic Acid. *Angew. Chemie Int. Ed.* **59**, 637–641 (2020).

45. Speidel, A. T. *et al.* Tailored Biocompatible Polyurethane-Poly(ethylene glycol) Hydrogels as a Versatile Nonfouling Biomaterial. *Adv. Healthc. Mater.* **11**, 2201378 (2022).

46. Kumari, S. *et al.* Thymol nanoemulsion exhibits potential antibacterial activity against bacterial pustule disease and growth promotory effect on soybean. *Sci. Reports 2018*

81 **8**, 1–12 (2018).

47. Lu, G. *et al.* Antibacterial thyme oil-loaded zwitterionic emulsion hydrogels. *J. Mater. Chem. B* **10**, 2691–2698 (2022).

48. Peng, J., Simon, J. R., Venema, P. & Van Der Linden, E. Protein Fibrils Induce Emulsion Stabilization. *Langmuir* **32**, 2164–2174 (2016).

49. Chen, M. H. *et al.* Methods to Assess Shear-Thinning Hydrogels for Application As Injectable Biomaterials. *ACS Biomater. Sci. Eng.* **3**, 3146–3160 (2017).

50. Huan, S., Ajdary, R., Bai, L., Klar, V. & Rojas, O. J. Low Solids Emulsion Gels Based on Nanocellulose for 3D-Printing. *Biomacromolecules* **20**, 635–644 (2019).

51. Bettio, L. E. B., Gil-Mohapel, J. & Rodrigues, A. L. S. Guanosine and its role in neuropathologies. *Purinergic Signal. 2016 123* **12**, 411–426 (2016).

52. Bai, L., Huan, S., Rojas, O. J. & McClements, D. J. Recent Innovations in Emulsion Science and Technology for Food Applications. *J. Agric. Food Chem.* **69**, 8944–8963 (2021).

53. Wang, C. *et al.* Temperature-responsive Pickering high internal phase emulsions for recyclable efficient interfacial biocatalysis. *Chem. Sci.* **13**, 8766–8772 (2022).

54. Solra, M., Das, S., Srivastava, A., Sen, B. & Rana, S. Temporally Controlled Multienzyme Catalysis Using a Dissipative Supramolecular Nanozyme. *ACS Appl. Mater. Interfaces* **14**, 45096–45109 (2022).

55. Wei, H., Cui, J., Lin, K., Xie, J. & Wang, X. Recent advances in smart stimuli-responsive biomaterials for bone therapeutics and regeneration. *Bone Res. 2022 101* **10**, 1–19 (2022).

56. Mura, S., Nicolas, J. & Couvreur, P. Stimuli-responsive nanocarriers for drug delivery. *Nat. Mater. 2013 1211* **12**, 991–1003 (2013).

57. Shi, Q. *et al.* Bioactuators based on stimulus-responsive hydrogels and their emerging biomedical applications. *NPG Asia Mater. 2019 111* **11**, 1–21 (2019).

58. Kalepu, S. & Nekkanti, V. Insoluble drug delivery strategies: review of recent advances and business prospects. *Acta Pharm. Sin. B* **5**, 442–453 (2015).

59. Yang, X. C. *et al.* Drug Delivery Using Nanoparticle-Stabilized Nanocapsules. *Angew. Chemie Int. Ed.* **50**, 477–481 (2011).

60. Xu, M. *et al.* Robust and highly adaptable high internal phase gel emulsions stabilized solely by a natural saponin hydrogelator glycyrrhizic acid. *Food Funct.* **13**, 280–289 (2022).

61. Tan, H., Sun, G., Lin, W., Mu, C. & Ngai, T. Gelatin particle-stabilized high internal phase emulsions as nutraceutical containers. *ACS Appl. Mater. Interfaces* **6**, 13977–13984 (2014).

62. Chen, W. H., Vázquez-González, M., Zoabi, A., Abu-Reziq, R. & Willner, I. Biocatalytic cascades driven by enzymes encapsulated in metal–organic framework nanoparticles. *Nat. Catal. 2018 19* **1**, 689–695 (2018).

63. Li, J. *et al.* Synthesis of many different types of organic small molecules using one automated process. *Science (80-.).* **347**, 1221–1226 (2015).

64. Martin, N. *et al.* Antagonistic chemical coupling in self-reconfigurable host–guest

protocells. *Nat. Commun. 2018 91* **9**, 1–12 (2018).

65. Sun, Z. *et al.* Enzyme–Polymer Conjugates as Robust Pickering Interfacial Biocatalysts for Efficient Biotransformations and One-Pot Cascade Reactions. *Angew. Chemie Int. Ed.* **57**, 13810–13814 (2018).

66. Namivandi-Zangeneh, R., Wong, E. H. H. & Boyer, C. Synthetic Antimicrobial Polymers in Combination Therapy: Tackling Antibiotic Resistance. *ACS Infect. Dis.* **7**, 215–253 (2021).

67. Ali, S. R., Pandit, S. & De, M. 2D-MoS2-based β-lactamase inhibitor for combination therapy against drug-resistant bacteria. *ACS Appl. Bio Mater.* **1**, 967–974 (2018).

68. Wu, H. *et al.* Synergistic Cisplatin/Doxorubicin Combination Chemotherapy for Multidrug-Resistant Cancer via Polymeric Nanogels Targeting Delivery. *ACS Appl. Mater. Interfaces* **9**, 9426–9436 (2017).

69. Mohamed, S. H., Mohamed, M. S. M., Khalil, M. S., Azmy, M. & Mabrouk, M. I. Combination of essential oil and ciprofloxacin to inhibit/eradicate biofilms in multidrug-resistant Klebsiella pneumoniae. *J. Appl. Microbiol.* **125**, 84–95 (2018).

……
……